ap
Asian Journal of Physics Vol. 24, No 4 (2015) 00-00

Optical biosensors exploiting the phenomenon of surface plasmon resonance

M A Baqir, Masih Ghasemi and P K Choudhury
Institute of Microengineering and Nanoelectronics, Universiti Kebangsaan Malaysia, UKM Bangi, 43600 Selangor, Malaysia

A prism-coupled waveguide biosensor is theoretically designed to determine the concentrations of the aqueous solutions of sugar, glycerol and potassium iodide. For this purpose, the principle of surface plasmon resonance (SPR) through the use of Turbadar-Kretschmann-Raether (TKR) configuration is exploited. The dips in reflection spectra, as generated due to the phenomenon of SPR, determine the levels of concentration of the measurands used. Moreover, the sensitivity of sensor system is analyzed corresponding to two different wavelengths, by taking into account water as the reference medium. The results essentially determine the efficacy of the TKR-based system in health diagnostics.

Keywords: SPR; prism-coupled optical sensor; optical biosensor

1 Introduction

Surface plasmon resonance (SPR) has been one of the interesting phenomena in recent years. The phenomenon of SPR has been greatly exploited in versatile fascinating applications in integrated optics, energy harvesting, and pharmaceutical, chemical and bio-related industries [1–7]. SPR results due to the oscillations of electrons in the conduction band, which is mostly attained at the interface of a thin metallic film having negative permittivity ($\mathrm{Re}(\varepsilon) < 0$) and a dielectric film having positive permittivity ($\mathrm{Re}(\varepsilon) > 0$). It takes place at the sub-wavelength scale, if the frequency of the incident light matches with the natural frequency of surface electrons, which oscillate against the restoring force [8–10]. In most of the SPR related cases, the incident light is totally absorbed, which is used for the oscillations of surface electrons, thereby causing the reflectivity to drop close to zero. As such, the phenomenon of SPR occurs when the wavenumber of the incident light matches with the surface plasmonic wavenumber.

Optical sensing has been one of the important areas wherein the exploitation of the phenomenon of SPR has been greatly dealt with. This is because the sensitivity of sensor is considerably enhanced in this case, and the phenomenon becomes worthwhile for sensing biomaterials and biogases [11–15]. For example, the technique of SPR is efficiently used to analyze bio-molecular interactions, legends, and chemical reactions. Also, SPR has many useful applications in our everyday life, such as food safety measurements and medical diagnosis [16–18]. Ref [19] show that the SPR-based sensors are used to detect living cells. Refs [20,21] demonstrate that chiral sculptured thin films (STFs) allow to generate multiple surface plasmon polaritons that can be used for sensing applications. Apart from these, the technique of SPR has also been of great demand for harvesting solar energy because plasmonic-based devices are used as wide band perfect absorbers [22,23], which absorb ultraviolet, visible and infrared light for solar heater applications.

The conditions of SPR remain extremely dependent on the alterations in the ambience. In optics, it is the refractive index (RI) value of the dielectric medium that governs the generation of the SPR – the feature basically used for optical sensing. A change in RI essentially alters the wavenumber of surface plasmonic waves, thereby altering the resonance condition. Furthermore, the operation of SPR-based sensors greatly depends on the modulation of wavelength, angle of incidence, intensity and phase of the incoming light.

Within the context, the most common approach to exploit the phenomenon of SPR, through the incorporation of metal-dielectric interface, has been the prism-coupled system, called as the Turbadar-Kretschmann-Raether (TKR) configuration [24,25] because of its being cheap and having easy setup. In the present communication, implementing the TKR configuration, we study the concentration of sugar,

Corresponding author :
e-mail: pankaj@ukm.edu.my; Phone: +60389118556; (P K Choudhury)

glycerol and potassium iodide solutions through developing the theory of waves in multilayered mediums in the presence of metal. The aforementioned measurands are taken into account as the presence and/or the absence of these leave great impact in determining human health related issues. As such, sensing the level of presence of these in human beings is often extremely important. In the present communication, the effect due to the thickness of the metallic layer is emphasized.

2 Treatment

Figure 1 illustrates the schematic diagram of prism-coupled optical biosensor configuration, wherein, in terms of the variation of RI, there exist five different layers from the bottom to the top. Initially, a thin layer (of nanoscale dimension) of silver is considered to be deposited over glass substrate, and the measurand is put above the metallic layer. The light is allowed to fall upon the metal-dielectric interface through a 45°-angled prism, which is mounted on the other side of glass substrate. As such, from the bottom to the top, the prism is having the RI n_1, the second layer of glass (of thickness d_1) is having the RI n_2, the third metallic nanolayer of silver has the RI as n_3 and the thickness d_2, and the measurand constitutes the fourth layer, of which the RI is taken to be n_4 and the thickness as d_3. The ambience above the measurand is essentially the free-space. In this configuration, the silver nanolayer is dispersive in nature, and its effective RI is altered by varying the wavelength λ_0 of the incidence light. The RI of metal can be defined as

$$n = \sqrt{\varepsilon_r + \varepsilon_i} = n_r + n_i \tag{1}$$

where ε_r and ε_i are, respectively, the real and the imaginary parts of permittivity of metal, whereas n_r and n_i are the respective real and the imaginary parts of the RI.

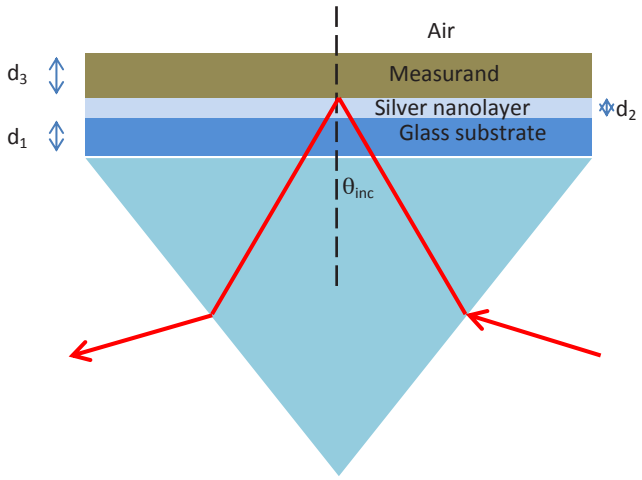

Fig 1. Schematic of TKR configuration used for sensing measurands.

Following Fig 1, the incident light of certain angle of incidence excites plasmonic waves, which can propagate along the metal-dielectric (or measurand) interface. The wave vector through the different interfaces of the illustrated sensor configuration can be expressed as [26]

$$k_{zi} = \frac{2\pi}{\lambda_0}\sqrt{n_i^2 - n_p^2 \sin\theta_{inc}} \tag{2}$$

with $i = 2, 3, 4$. In Eq (2), θ_{inc} is the angle of incidence (of the plane wave), k_{zi} is the wavenumber, n_p is the prism RI, and λ_0 is the free-space wavelength.

The surface reflectivity in the case of monolayer metallic thin film can be expressed as [15]

$$R = \frac{\gamma_{pm} + \gamma_{ms} \exp(2ik_m d_m)}{1 + \gamma_{pm}\gamma_{ms} \exp(2ik_m d_m)} \tag{3}$$

where k_m is the wavenumber in metal, d_m is the thickness of the metallic layer, and γ_{pm} and γ_{ms} are, respectively, Fresnel reflection coefficients for prism-metal and metal-sensing region layers. Now, the total reflectivity of prism can be estimated by adding the reflectivity values at the different interfaces [11], and written as

$$R = R_{12345} = \frac{\gamma_{12} + \mathrm{R}_{2345} \exp(2ik_{z1}d_1)}{1 + \gamma_{12}\mathrm{R}_{2345} \exp(2ik_{z1}d_1)} \tag{4}$$

with

$$R_{2345} = \frac{\gamma_{23} + R_{345} \exp(2ik_{z2}d_2)}{1 + \gamma_{23}R_{345} \exp(2ik_{z2}d_2)} \tag{5}$$

$$R_{345} = \frac{\gamma_{34} + \gamma_{45} \exp(2ik_{z3}d_3)}{1 + \gamma_{34}\gamma_{45} \exp(2ik_{z3}d_3)} \tag{6}$$

In the above set of equations d_1, d_2 and d_3 are, respectively, the thickness values of glass substrate, metal nanolayer and the measurand solution under examination, and k_{z1}, k_{z2} and k_{z3} are the normal components of wavevectors in glass substrate, silver nanolayer and measurand, respectively. Also, γ_{12}, γ_{23}, γ_{34} and γ_{45} are Fresnel reflection coefficients at the various medium interfaces, viz. prism-dielectric, dielectric-metal, metal-measurand and measurand-free-space boundaries.

Now, Fresnel reflection coefficients corresponding to the transverse electric (TE) and the transverse magnetic (TM) modes can be written as in [27]. Corresponding to the TE polarized wave, the reflection coefficient γ_{mn} assumes the form as

$$\gamma_{mn} = \frac{k_{zm} - k_{zn}}{k_{zm} + k_{zn}} \tag{7}$$

whereas for the TM polarized wave, it is as

$$\gamma_{mn} = \frac{\varepsilon_n k_{zm} - \varepsilon_m k_{zn}}{\varepsilon_n k_{zm} + \varepsilon_m k_{zn}} \tag{8}$$

In Eqs (7) and (8), m = 1,2,3 and n = 2,3,4.

In our SPR-based sensing configuration of Fig 1, the third (metallic) layer essentially has complex permittivity, which is frequency dependent, and can be determined by Drude-Lorentz model, described as

$$\varepsilon_{LD} = \varepsilon_L + \varepsilon_D \tag{9}$$

Drude model is also used to determine the dispersive properties of metal, and is expressed as

$$\varepsilon_D = 1 - \frac{f_1 \omega_p}{\omega(\omega - i\Gamma_1)} \tag{10}$$

In Eq (10), f_1 describes the oscillator strength, ω_p is the plasma frequency (that depends on the electron density and mass [26]), and Γ_1 is the scattering frequency arising due to electron-electron and/or electron-phonon interactions. The complex dielectric permittivity can be approximated by the use of Drude model [28], but its validity remains in limited range of wavelength. However, Drude model can be modified for its enhanced validity in terms of wavelength range by incorporating Lorentz model, expressed as

$$\varepsilon_L = \sum\nolimits_n \frac{f_n \omega_p}{\omega_n^{'2} \omega^2 + i\omega\Gamma_n^{'}} \tag{11}$$

with ω'_n and Γ'_n, respectively, as the oscillator frequency and the bandwidth, and f_n as the oscillator strength. The combination of Drude and Lorentz models would then yield the expression of complex permittivity [29] as

$$\varepsilon_D = 1 - \frac{f_1 \omega_p}{\omega(\omega - i\Gamma_1)} + \sum_n \frac{f_n \omega_p}{\omega_n'^2 \omega^2 + i\omega\Gamma_n'} \tag{12}$$

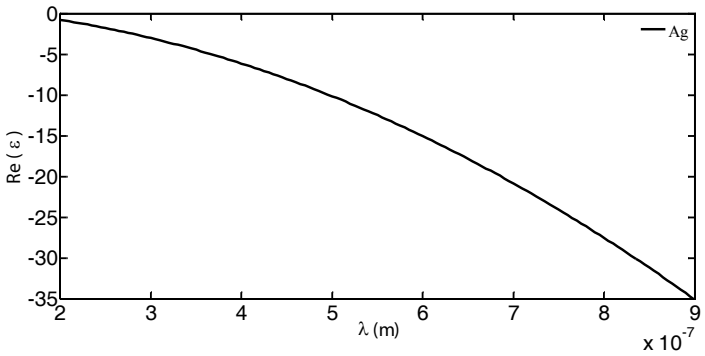

Fig 2a. The plot of Re(ε) against wavelength λ for silver metal.

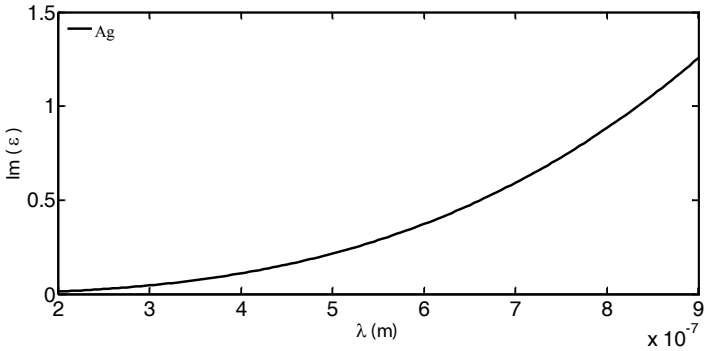

Fig 2b. The plot of Im(ε) against wavelength λ for silver metal.

Figure 2a illustrates the real part of the permittivity Re(ε) of silver in the selected range of wavelength, as achieved by using Drude-Lorentz model in Eq (12). From this figure, it becomes obvious that Re(ε) remains negative in the UV, visible and the IR regions of frequencies. Also, the magnitude of permittivity remains higher for the lower operating wavelength, and it lies in the range of −1 to −35 corresponding to the 200 − 900 nm wavelength range. Figure 2b shows the imaginary part Im(ε) of the permittivity of silver in the aforementioned range of operating wavelength. From this figure, we observe that the magnitude of Im(ε) is increased with the increase in wavelength. Furthermore, its value remains lower in the UV region and higher in the IR region.

3 Results and Discussion

We now analyze the sensing characteristics of the proposed sensor configuration. For this purpose, the complex permittivity of silver is determined by Drude-Lorentz model, which provides the approximate values that are close to the experimental ones. By the use of our model, we determine the concentrations of sugar, glycerol and potassium iodide at different wavelengths, taking into account two different values of thickness of silver layer. In the case of sugar solution, we used 441.5 nm, 532 nm and 635 nm as the

incident wavelengths, whereas for examining glycerol and potassium iodide, however, we considered 532 nm and 635 nm wavelengths only. We also determine the sensitivity of the proposed sensor configuration for different operating wavelengths. Furthermore, in our computations, we assume the thickness values of slab and solution (measurand) as 1000 nm each, whereas the RI values of prism and slab are taken as 2.70 and 1.44, respectively.

In order to achieve the phenomenon of SPR, the real part of the permittivity of metallic partner (of the interface) should be greater than the permittivity of the dielectric partner, and also, the permittivity value of metal should be negative in the operating wavelength range (as observed in Fig 2a). Furthermore, while using the TKR configuration, only the *p*-polarized light causes SPR.

We now focus on the attenuated total reflection (ATR) $\gamma = |R|^2$ patterns obtained for various forms of measurands that correspond to SPR upon the usage of the aforementioned TKR configuration. For illustrative examples, we use the aqueous solutions of sugar, glycerol and potassium iodide of different concentrations. Within the context, Table 1 shows the RI values of the aqueous solutions of sugar [30]. The motivation for considering sugar as an example is due to its emphatic role on determining human health because sugar is the source of energy used in many food products. However, the excess of sugar would cause chronic diseases such as diabetes mellitus. In medicinal area, it constitutes making oral rehydration solution (ORS) used to prevent children from diarrhea and vomiting. Apart from these, sugar is used in chemical industries for the production of cement, fabrics and surfactants [31].

Table 1. RI values of aqueous sugar solution of different concentrations, and the respective positions of reflectance minima corresponding to different values of incident light wavelength and metallic layer thickness.

% mass concentration of aqueous sugar soln.	RI values	Position of reflectance minima for θ_i (in degree)					
		λ = 441.5 nm		**λ = 532 nm**		**λ = 635 nm**	
		d		*d*		*d*	
		35 nm	**40 nm**	**35 nm**	**40 nm**	**35 nm**	**40 nm**
0	1.333	36.25	36.85	39.55	38.15	36.7	35.75
20	1.360	37	37.7	38.7	38.7	37.4	36.4
40	1.400	38.2	39	41.95	39.8	38.8	37.5

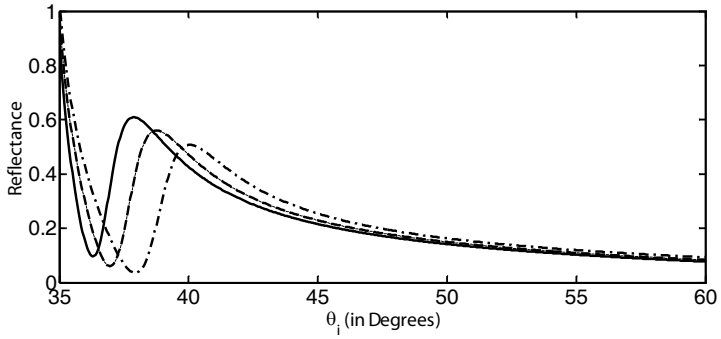

Fig 3 (a). ATR spectra for aqueous sugar solutions with the silver layer thickness as 35 nm and the incident light wavelength as 441.5 nm.

Figures 3a and 3b, respectively, demonstrate the ATR spectra obtained corresponding to the situations when the silver nanolayer assumes thickness values as 35 nm and 40 nm, and the incident light wavelength is as 441.5 nm; the angle of incidence is varied from 35° to 60°, in order to observe the effect due to the SPR which would result into maximum transmission of light (or the minimum reflection of it). In both the

figures, solid, dashed and dashed-dot lines correspond to 0%, 20% and 40% aqueous sugar solutions. We observe from Fig 3a that the minimum reflectivity for water (as the measurand) occurs at the incident angle 36.25°. With the increase in the concentration of sugar, a change in the RI value brings in alterations in the positions of reflectance minima, which may be used to determine the sugar level. However, a change in the thickness of the metallic layer also shifts the position of the reflectance minima by a very small amount, which is obvious from Fig 3b, obtained corresponding to the silver layer thickness as 40 nm. Apart from these, the increase of metallic layer thickness also reduces the reflectance minima a little, which is very much obvious.

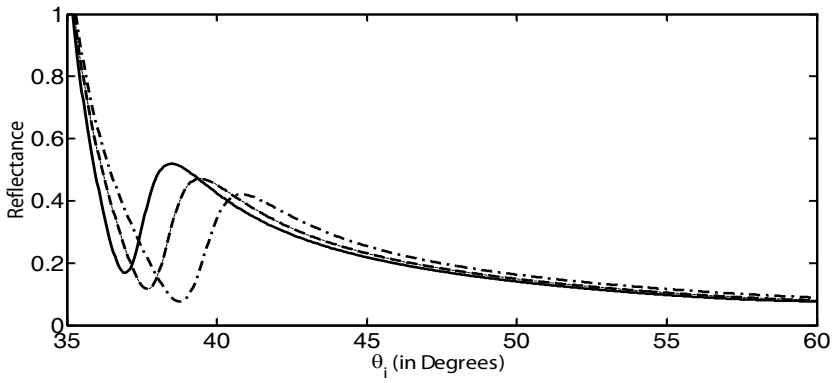

Fig 3b. ATR spectra for aqueous sugar solutions with the silver layer thickness as 40 nm and the incident light wavelength as 441.5 nm.

Upon altering the wavelength of the incident light to 532 nm, the ATR spectra get drastically altered, as can be seen in Figs 4a and 4b, obtained corresponding to the silver layer thickness values as 35 nm and 40 nm, respectively, in the configuration; the definition of three different curves in the plots are similar to as mentioned before. We observe that, corresponding to a 35 nm thickness of the metallic layer (Fig 4a), the reflectance minima for water (as the measurand) remains at 39.55°, and that shifts to 38.15° when a 40 nm thick metallic layer is used (Fig 4b). In both the situations (i.e. the two values of the metallic layer thickness), shifts in reflectance minima are clearly observed upon changing the concentration of sugar solution – the increase in concentration causes to obtain the reflectance minima at higher incidence angles – the feature that may be used for determining the concentration of measurand.

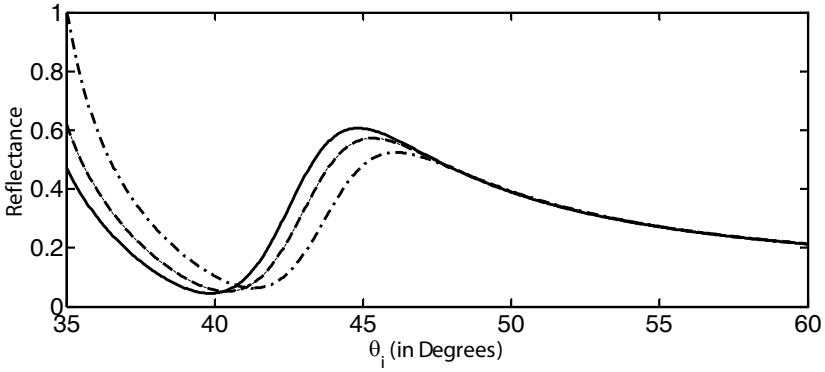

Fig 4a. ATR spectra for aqueous sugar solutions with the silver layer thickness as 35 nm and the incident light wavelength as 532 nm.

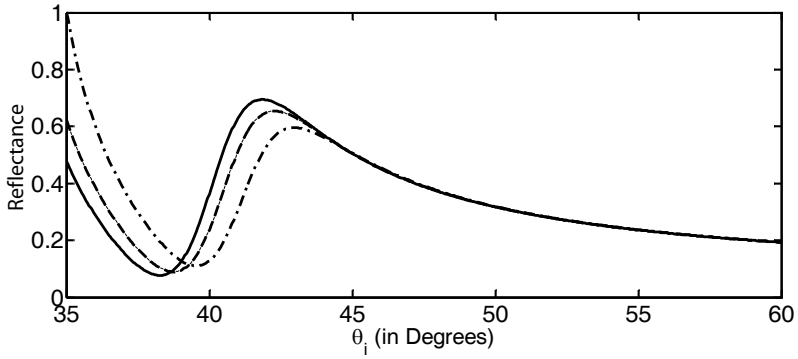

Fig 4b. ATR spectra for aqueous sugar solutions with the silver layer thickness as 40 nm and the incident light wavelength as 532 nm.

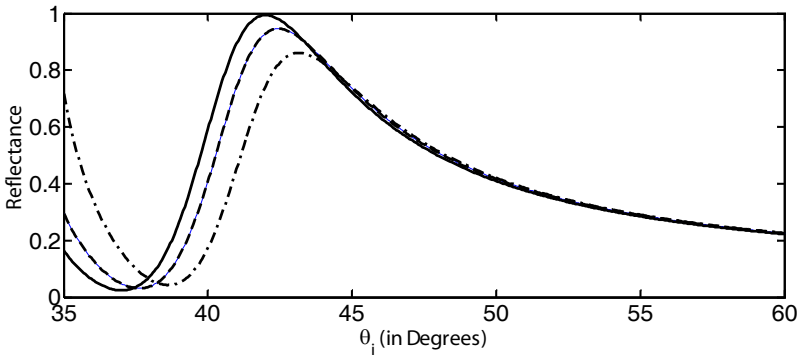

Fig 5a. ATR spectra for aqueous sugar solutions with the silver layer thickness as 35 nm and the incident light wavelength as 635 nm.

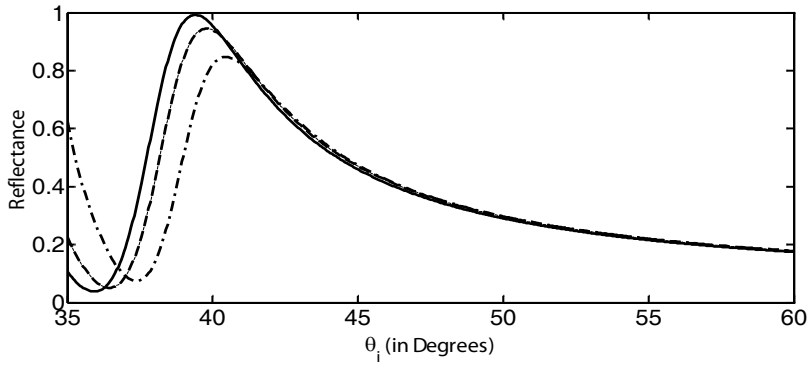

Fig 5b. ATR spectra for aqueous sugar solutions with the silver layer thickness as 40 nm and the incident light wavelength as 635 nm.

For the similar values of silver nanolayer thickness, as used above, making the incidence wavelength as 635 nm further alters the positions of the reflectance minima corresponding to the different values of concentration of sugar solutions, as can be seen in Figs 5a and 5b. In these figures too, the effect due to changes in metallic layer thickness is clearly observed; the curves correspond to the similar situations (in

respect of measurand concentrations) as stated before. All the results in respect of the angular shift of the reflectance minima corresponding to various situations are summarized in Table 1.

We consider glycerol as the next example of measurand, which is a naturally occurring chemical used as medicine. The intake of glycerol through mouth causes weight loss and enhances the performance of physical exercise. In diarrhea and vomiting, glycerol is used to reduce the loss of water from human body. Furthermore, glycerol is used in eyes before examination, in order to reduce pressure on cornea. Apart from these, it is used for moisturizing the skin and for laxation [32]. Table 2 presents the RI values of the aqueous solutions of glycerol with different mass concentrations [30].

Table 2. RI values of aqueous glycerol solution of different concentrations, and the respective positions of reflectance minima corresponding to different values of incident light wavelength and metallic layer thickness.

% mass concentration of aqueous glycerol soln.	RI values	Position of reflectance minima for θ_i (in degree)			
		λ = 532 nm		**λ = 635 nm**	
		d		*d*	
		35 nm	**40 nm**	**35 nm**	**40 nm**
0	1.333	39.55	38.15	36.7	35.75
10	1.347	40.15	38.4	37.1	36.1
15	1.357	40.5	38.8	37.55	36.3

Figures 6a and 6b, respectively, illustrate the reflectance characteristics of the aqueous solutions of glycerol under the assumption of the operating wavelength as 532 nm, and the silver nanolayer thickness values as 35 nm and 40 nm. The solid, dashed and dashed-dot lines in these figures correspond to the cases of 0% (i.e. water as measurand), 10% and 15% aqueous solutions of the measurand. We observe from Fig 6a that the use of water as measurand yields the reflectance minima at the value of the angle of incidence as 39.55°, and the increase in measurand concentration shifts the positions of the reflectance minima to the larger values of the incidence angle. For example, 10% aqueous solution of glycerol results in the position of reflectance minima (due to the generation of SPR) at an angle 40.15°, whereas 15% solution shows the minima at 40.5°. The results corresponding to the increased value of metallic nanolayer thickness are illustrated in Fig 6b, which clearly shows shift in the position of reflectance minima in this case toward the lower values of the incidence angle, and thereby demonstrates the effect on the SPR due to the structure of the metallic partner of the interface.

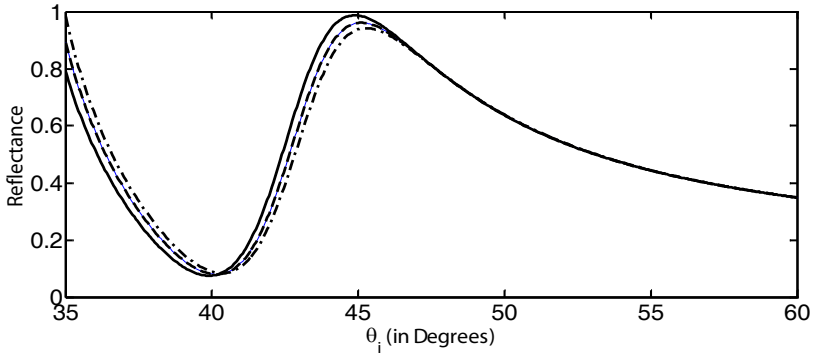

Fig 6a. ATR spectra for aqueous glycerol solutions with the silver layer thickness as 35 nm and the incident light wavelength as 532 nm.

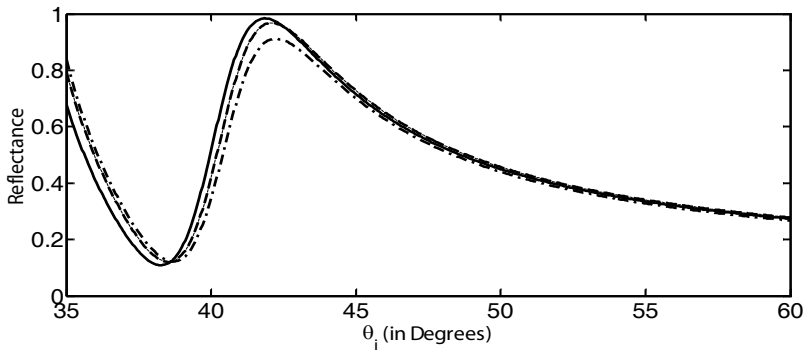

Fig. 6b. ATR spectra for aqueous glycerol solutions with the silver layer thickness as 35 nm and the incident light wavelength as 532 nm.

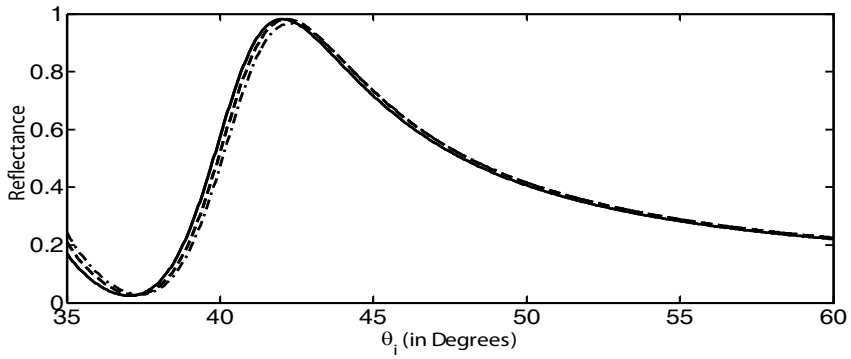

Fig 7a. ATR spectra for aqueous glycerol solutions with the silver layer thickness as 35 nm and the incident light wavelength as 635 nm.

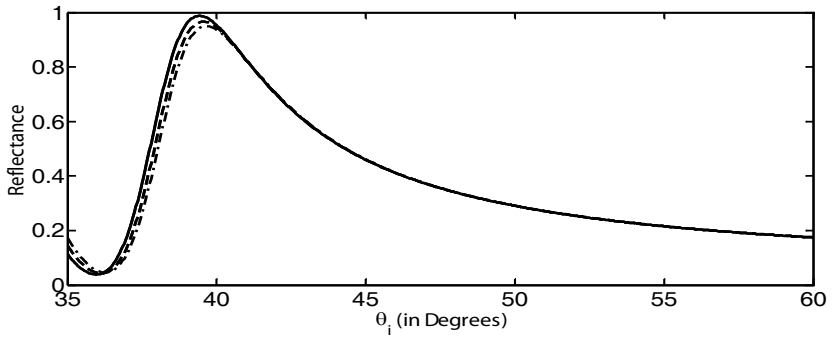

Fig 7b. ATR spectra for aqueous glycerol solutions with the silver layer thickness as 40 nm and the incident light wavelength as 635 nm.

Figures 7a and 7b, obtained for the two values of metallic nanolayer thickness, viz. 35 nm and 40 nm, respectively, correspond to the situation when the incidence light wavelength is taken as 635 nm. We observe that the increase in incidence wavelength causes to shift the reflectance minima toward the lower values of the incidence angle. Also, similarly to what observed before, the increase in measurand concentration increases the angular position of the reflectance dip. Increase in metallic layer thickness too

significantly affects the reflectance spectrum, which becomes very much obvious upon comparing Figs 7a and 7b. The dependence of spectral characteristics on the metallic layer thickness as well as the measurand concentration is summarized in Table 2.

Table 3. RI values of aqueous potassium iodide solution of different concentrations, and the respective positions of reflectance minima corresponding to different values of incident light wavelength and metallic layer thickness.

% mass concentration of aqueous potassium iodide soln.	RI values	Position of reflectance minima for θ_i (in degree)			
		λ = 532 nm		**λ = 635 nm**	
		d		***d***	
		35 nm	**40 nm**	**35 nm**	**40 nm**
0	1.333	39.55	38.15	36.7	35.75
10	1.3469	40.1	38.6	37.2	36.15
30	1.3801	40.95	39.3	38	36.7

Considering potassium iodide as another example of measurand, Table 3 provides the information of the RI dependence on the concentration of potassium iodide solution [33]; percentage mass concentration of the aqueous solution of potassium iodide is taken into account. The reason behind choosing potassium iodide remains due to its enormous importance in medicinal applications/diagnostics. For example, it is greatly used in radiation exposure emergency to protect thyroid glands in human beings from absorbing radioactive iodine, and eventually to reduce the risk due to thyroid cancer. Further, potassium iodide is used to treat overactive thyroid glands. Apart from these, potassium iodide has many side effects, e.g. the excess of potassium iodide causes fever, diarrhea, swelling in throat etc. [34].

We take into account 0%, 10% and 30% aqueous solutions of potassium iodide to sense by the use of TKR configuration, and in this case too, we make attempts to observe the ATR spectra under 532 nm and 635 nm wavelengths. Also, similarly to the previous situations, we consider the thickness values of metallic nanolayer as 35 nm and 40 nm. The obtained results are shown in Figs 8 and 9 corresponding to the silver layer thickness as 35 nm and 40 nm.

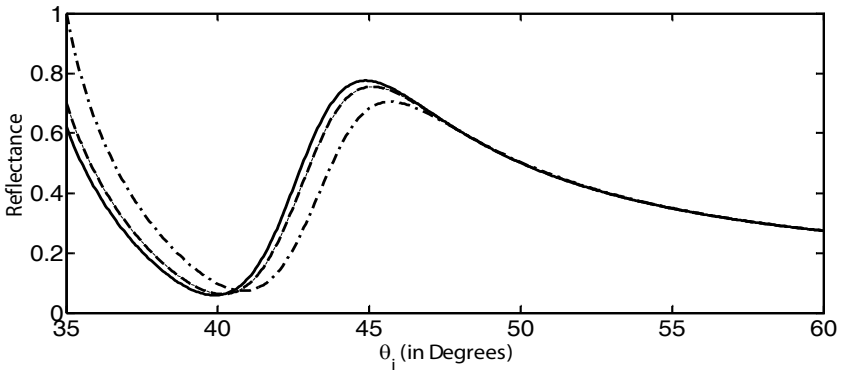

Fig. 8a. The ATR spectra for aqueous potassium iodide solutions with the silver layer thickness as 35 nm and the incident light wavelength as 532 nm.

Upon comparing Figs 8a and 8b, we clearly observe that, similarly to the previous cases, the increase of the thickness of silver nanolayer results in shift of the position of reflectance minima towards lesser values of the angle of incidence. We find from Fig 8a that 0%, 10% and 30% aqueous solutions of potassium iodide yield the reflectance minima at the angles of incidence values as 39.55°, 40.1° and 40.95°, respectively, corresponding to the situation when the metallic nanolayer thickness is taken as 35 nm. Upon

increasing the thickness to 40 nm, the respective positions of the reflectance minima occur at 38.15°, 38.6° and 39.3°. We generally observe in all the situations that the increase of the thickness of the metallic partner in the TKR configuration fairly makes the ATR spectra sharper.

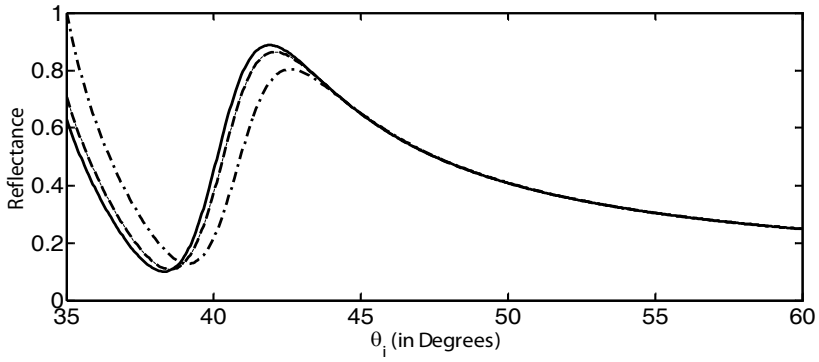

Fig 8b. The ATR spectra for aqueous potassium iodide solutions with the silver layer thickness as 40 nm and the incident light wavelength as 532 nm.

As stated before, the plots illustrated in Figs 9a and 9b correspond to 635 nm operating wavelength. Comparing Figs 8 and 9, we find that the increase of wavelength results in the shift of the reflectance minima to lower values of the angle of incidence. Further, it is clear from Figs 9a and 9b that, for both the values of metallic layer thickness, the variations in the concentration of measurand cause shifts in the positions of the reflectance minima, which can be read to determine the characteristics of the measurand. All the results obtained in Figs 8 and 9 are tabulated in Table 3 to have a cursory look at the shifts in the angle of incidence that cause the phenomenon of SPR to take place.

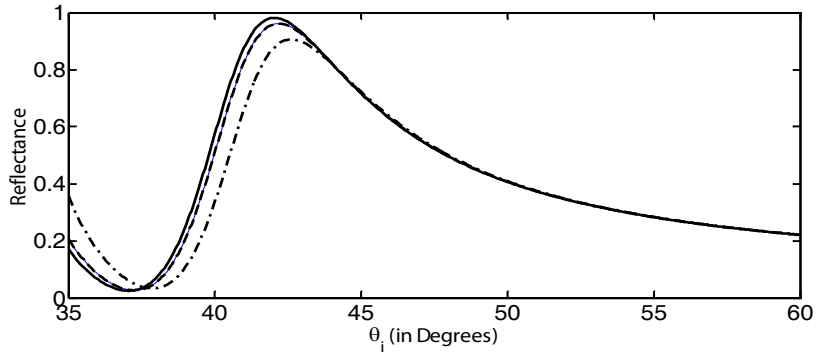

Fig 9a. The ATR spectra for aqueous potassium iodide solutions with the silver layer thickness as 35 nm and the incident light wavelength as 635 nm.

It remains obvious from the aforementioned description that the configuration is used as sensing the measurand. Within the context, to determine the sensitivity of the system remains very important which, in the present case, is defined in terms of the angular shift in the reflectance minima upon varying the RI of the medium with respect to aqua. As such, if the RI of the solution under examination is n_s and the RI of water is n_w, the sensitivity can then be defined as [14]

$$S = \frac{\theta_s - \theta_w}{n_s - n_w} \tag{13}$$

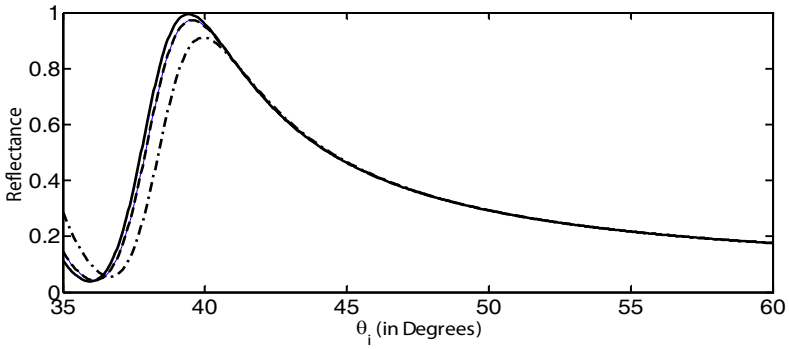

Fig 9b. The ATR spectra for aqueous potassium iodide solutions with the silver layer thickness as 40 nm and the incident light wavelength as 635 nm.

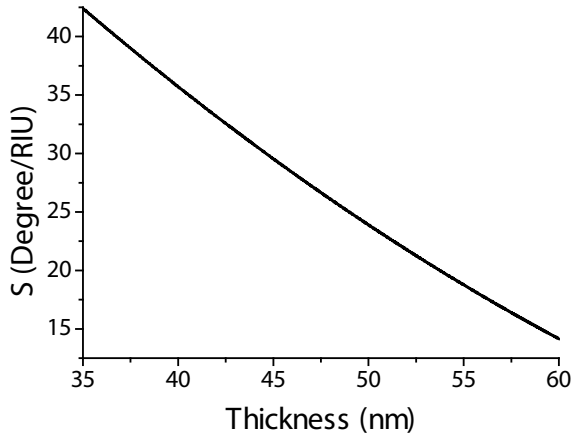

Fig 10. Plot of sensitivity S against metallic nanolayer thickness corresponding to 532 nm wavelength.

In Eq (13), θ_s is the angle of incidence at which the SPR is achieved while the measurand is in use, θ_w is the incident angle at which the SPR is observed, taking into account water as the reference medium.

As the metallic layer used in the sensor configuration essentially has its great impact on the generation of the phenomenon of SPR, depending on the results obtained above, we plot the variation of sensitivity against the thickness of the metallic layer. Also, we use the results obtained by taking into account the incidence wavelengths as 532 nm and 635 nm. In this stream, Figs 10 and 11, respectively, illustrate the dependence of sensitivity on the thickness of silver nanolayer corresponding to 532 nm and 635 nm operating wavelengths.

We observe from Figs 10 and 11 that the sensitivity decreases almost linearly with the increase in metallic nanolayer thickness; the linearity remains more maintained corresponding to 532 nm wavelength. With the higher value of operating wavelength, the decrease in sensitivity becomes exponential more toward the higher value of metallic layer thickness. The decrease in sensitivity with increasing thickness is very much expected as the phenomenon of SPR greatly depends on the metallic partner of the interface – the thinner the layer is, the easier will be the excitation of electrons from the surface of metal, which take part in the plasmonic resonance event. As we used the values of silver nanolayer thickness as 35 nm and 40 nm, we notice from Fig 10 that, corresponding to 532 nm incidence wavelength, the respective sensitivity values are 42 °/RIU and 36 °/RIU. Further, corresponding to these two thickness values, the use of 635 nm yields the respective sensitivity values as 44 °/RIU and 35 °/RIU (Fig 11). Though the difference in the

values of sensitivity for the two different types of wavelengths is not significant enough, the measurand (or the dielectric partner of the interface) remains another determining factor in this regard.

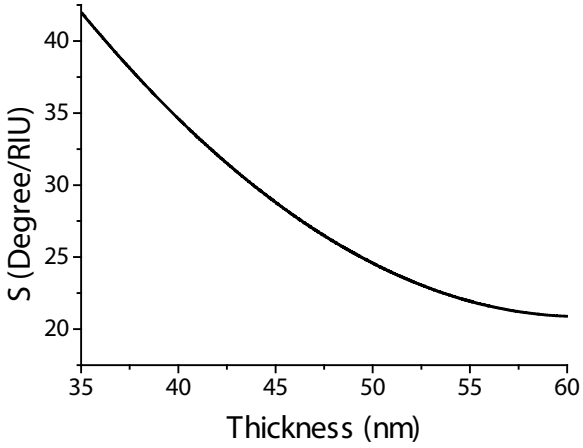

Fig 11. Plot of sensitivity S against metallic nanolayer thickness corresponding to 635 nm wavelength.

4 Conclusions

The aforementioned discussions essentially focus on the SPR-based sensing of a few exemplified measurands by the use of TKR configuration. It has been observed that the ATR spectra of measurands essentially depend on the thickness of the metallic partner in the process of SPR, and also, the operating wavelength. The concentration of measurand remains responsible for attaining the reflectance minima, and the shifts in its position. It has been found that the increase in metallic nanolayer thickness shifts the reflectance minima to lower values of the incidence angle. Also, the increase in wavelength too similarly results for attaining the reflectance dip. The results indicate that small change in the concentration of solution can be sensed, and the sensor can be used for chemical and pharmaceutical applications. Finally, attempts have been made to demonstrate the usefulness of TKR configuration in medical diagnostics through sensing the presence of (toxic) elements that are (possibly) hazardous for human health.

Acknowledgments

The authors are thankful to the Ministry of Higher Education (Malaysia) to support the work through the Hi-COE grant AKU-95.

References

1. Liedberg B, Nylander C, Surface plasmon resonance for gas detection and biosensing, *Sens and Actuat*, 4(1983)299-304.
2. Lal S, Link S, Halas N J, Nano-optics from sensing to waveguiding, *Nat Photon*, 1(2007)641-648.
3. Oulton R F, Bartal G, Pile DFP, Zhang X, Confinement and propagation characteristics of subwavelength plasmonic modes, *New J Phys,* 10(2008)105018-1-105018-14.
4. Schuller J A, Barnard E S, Cai W, Jun Y C,White J S, Brongersma M L, Plasmonics for extreme light concentration and manipulation, *Nat Mater*, 9(2010)193-204.
5. Thillaivinayagalingam P, Gommeaux J, McLoughlin M, Collins D, Newcombe A R, Biopharmaceutical production: applications of surface plasmon resonance biosensors, *J Chromatog B*, 878(2010)149-153.
6. Abbas A, Linman M J, Cheng Q, New trends in instrumental design for surface plasmon resonance-based biosensors, *Biosens and Bioelectron*, 26(2011)1815-1824.
7. Li Y, Xu L, Li B, Gold nanorod-induced localized surface plasmon for microparticle aggregation, *Appl Phys Lett*, 101(2012)053118-1-053118-3.

8. Plotz G A, Simon H J, Tucciarone J M, Enhanced total reflection with surface plasmons, *J Opt Soc Am*, 69(1979)419-422.
9. Berini P, Long-range surface plasmonpolaritons, *Adv in Opt and Photon*, 1(2009)484-588.
10. Kristjan L, Optical amplification of surface plasmon polaritons: Review, *J Nanophoton*, 6(2012)061801-1-061801-9.
11. Zhang H F, Wang Q, Shen N H, Li R, Chen J, Ding J, Wang H T, Surface Plasmon polaritons at interfaces associated with artificial composite materials, *J Opt Soc Am B*, 22(2005)2686-2696.
12. Zayats A V, Smolyaninov II, Maradudin A A, Nano-optics of surface plasmon polaritons, *Phys Repts*, 408(2005)131-314.
13. Liu X, Cao Z, Zhu P, Shen Q, Liu X, Large positive and negative lateral optical beam shift in prism-waveguide coupling system, *Phys Rev E*, 73(2006)056617-1-056617-5.
14. Wijaya E, Lenaerts C, Maricot S, Hastanin J, Habraken S, Vilcot J P, Boukherroub R, Szunerits S, Surface plasmon resonance-based biosensors: from the development of different SPR structures to novel surface functionalization strategies, *Curr Opin in Sol Stat and Mat Sci*, 15(2011)208-224.
15. Sharma A K, Jha R, Gupta B D, Fiber-optic sensors based on surface plasmon resonance: A comprehensive review, *IEEE Sensor J*, 7(2007)1118-1129.
16. Ladd J, Taylor A, Tiang S, SPR biosensors for food safety, *Springer Ser Chem Sen Biosen*, 4(2006)207-227.
17. Sonny S, Sesay A M, Virtanen V, Development of diagnostic SPR based biosensor for the detection of pharmaceutical compounds in saliva, *Proc SPIE*, 7376(2010)737605-1-737605-6.
18. Olaru A, Bala C, Jaffrezic-Renault N, Aboul-Enein H Y, Surface plasmon resonance (SPR) biosensors in pharmaceutical analysis, *Critical Rev in Anal Chem*, 45(2015)97-105.
19. Yanase Y, Hiragun T, Ishii K, Kawaguchi T, Yanase T, Kawai M, Sakamoto K, Hide M, Surface plasmon resonance for cell-based clinical diagnosis, *Sensors*, 14(2014)4948-4959.
20. Mackay T G, Lakhtakia A, Modeling chiral sculptured thin film as platform for surface-plasmonic-polaritonic optical sensing, *IEEE Sensor J*, 12(2012)273-280.
21. Abbas F, Lakhtakia A, Naqvi Q A, Faryad M, An optical-sensing modality that exploits Dyakonov-Tamm waves, *Phot Res*, 3(2015)5-8.
22. Okamoto T,Yamaguchi I. Absorption measurement using a leaky waveguide mode, *Opt Rev*, 4(1997)354-357.
23. Cao T, Wei CW, Simpson RE, Zhang L, Cryan MJ. Broadband polarization-independent perfect absorber using a phase-change metamaterial at visible frequencies, *Sci Rept*, 4(2014)3955-1-3955-8.
24. Turbadar T, Complete absorption of light by thin films, *Proc Phys Soc, Lond*, 73(1959)40-44.
25. Kretschmann E, Raether H, Radiative decay of nonradiative surface plasmons excited by light, *Z Naturforsch A*, 23(1968)2135-2136.
26. Palik E D, Handbook of Optical Constants of Solids, (Acadmic Press: New York, NY), 1998.
27. Raether H, Surface Plasmon on Smooth and Rough Surfaces and on Gratings, Springer Tracts in Mod Phys, vol. 111, (Springer: Berlin), 1988.
28. Li H Y, Zhou S M, Li J, Chen Y L, Wang S Y, Shen Z C, Chen L Y, Liu H, Zhang X X, Analysis of the Drude model in metallic films, *Appl Opt*, 40(2001)6307-6311.
29. Rakić A D, Djurišić A B, Elazar J M, Majewski M L, Optical properties of metallic films for vertical-cavity optoelectronic devices, *Appl Opt*, 37(1998)5271-5283.
30. Astle R C, Weast M J, Handbook of Chemistry and Physics, 64th Edition, (Boca Raton: CRC Press), 1984.
31. Pereira M A, The possible role of sugar-sweetened beverages in obesity etiology: a review of the evidence, Int J Obesit, 30(2006)S28-S36.
32. Tan W H, Aziz ARA, Aroua M K, Glycerol production and its applications as a raw material: A review, *Renew and Sust Energy Rev*, 27(2013)118-127.
33. Söhnel O, Novotny P, Densities of Aqueous of Inorganic Substances, (Elsevier: New York, NY), 1985.
34. Costa R O, de Macedo P M, Carvalhal A, Bernardes-Engemann A R, Use of potassium iodide in dermatology: updates on an old drug, *An Bras Dermatol*, 88(2013)396-402.

[*Received*: 17. 4. 2015]